

1-1-2004

## All-optical modulation in dye-doped nematic liquid crystal photonic bandgap fibers

Thomas Tanggard Alkeskjold

Jesper Laegsgaard

Anders Bjarklev

David Sparre Hermann

Jes Broeng

*See next page for additional authors*

Find similar works at: <https://stars.library.ucf.edu/facultybib2000>

University of Central Florida Libraries <http://library.ucf.edu>

This Article is brought to you for free and open access by the Faculty Bibliography at STARS. It has been accepted for inclusion in Faculty Bibliography 2000s by an authorized administrator of STARS. For more information, please contact [STARS@ucf.edu](mailto:STARS@ucf.edu).

---

### Recommended Citation

Alkeskjold, Thomas Tanggard; Laegsgaard, Jesper; Bjarklev, Anders; Hermann, David Sparre; Broeng, Jes; Li, Jun; and Wu, Shin-Tson, "All-optical modulation in dye-doped nematic liquid crystal photonic bandgap fibers" (2004). *Faculty Bibliography 2000s*. 4180.

<https://stars.library.ucf.edu/facultybib2000/4180>

---

**Authors**

Thomas Tanggard Alkeskjold, Jesper Laegsgaard, Anders Bjarklev, David Sparre Hermann, Jes Broeng, Jun Li, and Shin-Tson Wu

# All-optical modulation in dye-doped nematic liquid crystal photonic bandgap fibers

Thomas Tangaard Alkeskjold, Jesper Lægsgaard and Anders Bjarklev

COM Center, Technical University of Denmark, DK-2800 Lyngby, Denmark.  
[tl@com.dtu.dk](mailto:tl@com.dtu.dk), [jl@com.dtu.dk](mailto:jl@com.dtu.dk), [ab@com.dtu.dk](mailto:ab@com.dtu.dk)

David Sparre Hermann and Anawati

Photonics Laboratory, Department of Microtechnology and Nanoscience MC2, Chalmers University of Technology,  
412 96 Gothenburg, Sweden.  
[David.Hermann@mc2.chalmers.se](mailto:David.Hermann@mc2.chalmers.se)

Jes Broeng

Crystal Fibre A/S, Blokken 84, DK-3460 Birkerød, Denmark  
[jb@crystal-fibre.com](mailto:jb@crystal-fibre.com)

Jun Li and Shin-Tson Wu

College of Optics and Photonics: CREOL & FPCE, University of Central Florida, Orlando, Florida 32816, USA  
[junli@mail.ucf.edu](mailto:junli@mail.ucf.edu), [swu@mail.ucf.edu](mailto:swu@mail.ucf.edu)

**Abstract:** Photonic crystal fibers (PCFs) have attracted significant attention during the last years and much research has been devoted to develop fiber designs for various applications, hereunder tunable fiber devices. Recently, thermally and electrically tunable PCF devices based on liquid crystals (LCs) have been demonstrated. However, optical tuning of the LC PCF has until now not been demonstrated. Here we demonstrate an all-optical modulator, which utilizes a pulsed 532nm laser to modulate the spectral position of the bandgaps in a photonic crystal fiber infiltrated with a dye-doped nematic liquid crystal. We demonstrate a modulation frequency of 2kHz for a moderate pump power of 2-3mW and describe two pump pulse regimes in which there is an order of magnitude difference between the decay times.

©2004 Optical Society of America

OCIS codes: (060.2310) Fiber optics, (230.3990) Microstructure devices

---

## References and Links

1. B. J. Eggleton, C. Kerbage, P. S. Westbrook, R. Windeler & A. Hale, "Microstructured optical fiber devices," *Opt. Express* **9**, 698-713 (2001), <http://www.opticsexpress.org/abstract.cfm?URI=OPEX-9-13-698>
2. R. T. Bise, R. S. Windeler, K. S. Kranz, C. Kerbage, B. J. Eggleton, and D. J. Trevor, "Tunable photonic band gap fiber," in *OSA Trends in Optics and Photonics (TOPS) 70, Optical Fiber Communication Conference Technical Digest, Postconference Edition (Optical Society of America, Washington, DC, 2002)*, 466-468.
3. T. T. Larsen, A. Bjarklev, D. S. Hermann, and J. Broeng, "Optical devices based on liquid crystal photonic bandgap fibres," *Opt. Express* **11**, 2589-2596 (2003).  
<http://www.opticsexpress.org/abstract.cfm?URI=OPEX-11-20-2589>
4. M. W. Haakestad, T. T. Larsen, M. D. Nielsen, H. E. Engan, and A. Bjarklev, "Electrically Tunable Fiber Device Based on a Nematic Liquid Crystal Filled Photonic Crystal Fiber," *ECOC 2004, postdeadline paper Th4.3.2, Stockholm, Sweden*.
5. F. Du, Y.Q. Lu and S.T. Wu, "Electrically tunable liquid-crystal photonic crystal fiber," *Appl. Phys. Lett.* **85**, 2181-2183 (2004).
6. P. G. de Gennes and J. Prost, *The Physics of Liquid Crystals*, 2nd edition, (Clarendon Press, Oxford, 1993).
7. Y.-J. Wang and G. O. Carlisle, "Optical properties of disperse-red-1-doped nematic liquid crystal," *J. Materials Science: Materials in electronics* **13**, 173-178 (2002).
8. J. Li and S.T. Wu, "Extended Cauchy equations for the refractive indices of liquid crystals," *J. Appl. Phys.* **95**, 896-901 (2004).

9. J. Li, S. Gauza and S. T. Wu, "Temperature effect on liquid crystal refractive indices," *J. Appl. Phys.* **96**, 19-24 (2004).
10. A. K. Abeeluck, N.M. Litchinitser, C. Headley and B. J. Eggleton, "Analysis of spectral characteristics of photonic bandgap waveguides," *Opt. Express* **10**, 1320-1333 (2002).  
<http://www.opticsexpress.org/abstract.cfm?URI=OPEX-10-23-1320>
11. N. M. Litchinitser, S. C. Dunn, P. E. Steinvurzel, B. J. Eggleton, T. P. White, R. C. McPhedran, and C. M. de Sterke, "Application of an ARROW model for designing tunable photonic devices," *Opt. Express* **12**, 1540-1550 (2004). <http://www.opticsexpress.org/abstract.cfm?URI=OPEX-12-8-1540>
12. J. Laegsgaard, "Gap formation and guided modes in photonic bandgap fibres with high-index rods," *J. Opt. A: Pure and Appl. Opt.* **6**, 798-804 (2004).
13. C. Hu and J. R. Whinnery, "Losses of a nematic liquid-crystal optical waveguide," *J. Opt. Soc. Am* **64**, 1424-1432 (1974).
14. M. Green and S. J. Madden, "Low loss nematic liquid crystal cored fiber waveguides," *Appl. Opt.* **28**, 5202-5203 (1989).
15. D. Ferrarini, L. Vincetti, M. Zoboli, A. Cucinotta, and S. Selleri, "Leakage properties of photonic crystal fibers," *Opt. Express* **10**, 1314-1319 (2002).  
<http://www.opticsexpress.org/abstract.cfm?URI=OPEX-10-23-1314>
16. N. A. Mortensen, "Effective area of photonic crystal fibers," *Opt. Express* **10**, 341-348 (2002),  
<http://www.opticsexpress.org/abstract.cfm?URI=OPEX-10-7-341>
17. J. Riishede, J. Laegsgaard, J. Broeng, and A. Bjarklev, "All-silica photonic bandgap fibre with zero dispersion and a large mode area at 730nm," *J. Opt. A: Pure Appl. Opt.* **6**, 667-670 (2004).
18. A. Ortigosa-Blanch, J. C. Knight, W. J. Wadsworth, J. Arriaga, B. J. Mangan, T.A. Birks, and P. St. J. Russell, "Highly birefringent photonic crystal fibers," *Opt. Lett.* **25**, 1325-1327 (2000).
19. J. R. Folkenberg, M. D. Nielsen, N. A. Mortensen, C. Jakobsen, and H. R. Simonsen, "Polarization maintaining large mode area photonic crystal fiber," *Opt. Express* **12**, 956-960 (2004),  
<http://www.opticsexpress.org/abstract.cfm?URI=OPEX-12-5-956>
20. D. Armitage and S. M. Delwart, "Nonlinear optical effects in the nematic phase," *Mol. Cryst. Liq. Cryst.* **122**, 59-75 (1985).
21. I. C. Khoo, *Liquid Crystals: Physical properties and nonlinear optical phenomena* (Wiley Interscience, New York, 1995).
22. D. Armitage, "Thermal properties and heat flow in the laser addressed liquid-crystal display," *J. Appl. Phys.* **52**, 1294-1300 (1981).

## 1. Introduction

Photonic crystal fibers (PCFs) have attracted significant attention during the last years and much research has been devoted to develop fiber designs for various applications, hereunder tunable fiber devices. This type of device was first demonstrated by Eggleton *et al.* [1], where a high-index liquid plug was dynamically positioned in a tapered 'grapefruit' fiber, thereby creating a fiber device with tunable transmission properties. Later, Bise *et al.* [2] demonstrated a tunable photonic bandgap fiber, where the air holes of a solid-core PCF were filled with a high-index oil. Recently, thermally tunable fiber devices based on Liquid Crystals (LCs) were presented [3], and tunable and switchable bandgaps were demonstrated. Recently, electrical control was achieved using external applied electric fields to reorient the LC [4,5]. In [4], the cladding holes of a solid core PCF were infiltrated with a LC and the LCPCF was placed between electrodes and the photonic bandgaps in the LC filled section could be electrically tuned. The reorientation of the LC by the E-field, resulted in a high anisotropy in the cross-section of the PCF, and a Polarization Dependent Loss (PDL) was introduced when the E-field was applied. No PDL was present when the E-field was off. A modulation frequency of 5Hz was demonstrated at  $\lambda=1500\text{nm}$ , and the rise and decay times were 5ms and 52ms, respectively. In [5], the core and cladding holes of an aircore photonic bandgap fiber were filled with a LC, which transformed the PBG guiding fiber into a TIR guiding fiber. The transmission of a 633nm HeNe laser could be switched by applying a voltage across the fiber and the rise and decay times were here 10ms and 200ms, respectively.

However, optical control of PCF properties has until now not been demonstrated. In this paper, we present an all-optical tunable Liquid Crystal Photonic BandGap (LCPBG) fiber device, which utilizes a pulsed 532nm laser to modulate the spectral position of the bandgaps in a PCF infiltrated with a dye-doped nematic liquid crystal. This device utilizes local heating of the LC to shift the spectral position of the bandgaps and introduces, in principle, no PDL. A modulation frequency of 2kHz is demonstrated for a pump power of 2-3mW.

## 2. The LCPBG fiber device

In this experiment we used a so-called ‘Large-Mode Area’ PCF, an all-silica PCF, which has a silica core surrounded by 7 periods of air holes arranged in a triangular lattice. The hole diameter, inter-hole distance and core size are  $3\mu\text{m}$ ,  $7\mu\text{m}$  and  $10\mu\text{m}$ , respectively. The fiber is endlessly single mode and guides light by the principle of modified Total-Internal-Reflection (mTIR). An optical micrograph of the end facet of the PCF is shown in Fig. 1(a). The fiber was infiltrated for 10mm of its length with a nematic Liquid Crystal (LC, Merck, E7) using capillary forces. Depending on the mesophase as well as the surface boundary conditions, the LC mesogens will align in a specific orientational configuration, which minimizes the free energy of the LC [6]. Using polarized microscopy on a  $5\mu\text{m}$  fused silica capillary tube, we found that E7 was aligned in a planar alignment, i.e., with the director of the LC pointing mainly along the fiber over the entire cross-section of the capillary. It is, therefore, reasonable to assume that this alignment is also present in the  $3\mu\text{m}$  tubes, which constitute the PCF. Figure 1(b) shows polarized micrographs of the  $5\mu\text{m}$  silica tube infiltrated with the LC in its nematic phase. The top picture is when the angle between the capillary axis and the crossed polarizers is  $0/90$  degrees and the bottom picture is when the angle is  $45$  degrees between the capillary and the polarizers. In addition, polarized microscopy investigations on another nematic liquid crystal, 5CB (one of the components of E7; see Fig. 2, top left), in fused silica tubes of  $6\mu\text{m}$  and  $2\mu\text{m}$  diameter, respectively, gave the same result concerning the alignment of the liquid crystal. In this study, the direction of the optic axis (the director) was further validated by observing the change of birefringence colors when inserting an additional  $\lambda/4$ -wave plate into the polarizing microscope after the capillary tube specimen, but before the crossed analyzer, and oriented at  $0/90$  degrees with respect to the axis of the capillary. In this way, it was possible to determine explicitly that the director was indeed parallel to the capillary tube axis, and not perpendicular to it. In addition, the uniformity of the alignment was greater in the  $2\mu\text{m}$  capillary tube than in the  $6\mu\text{m}$  capillary tube.

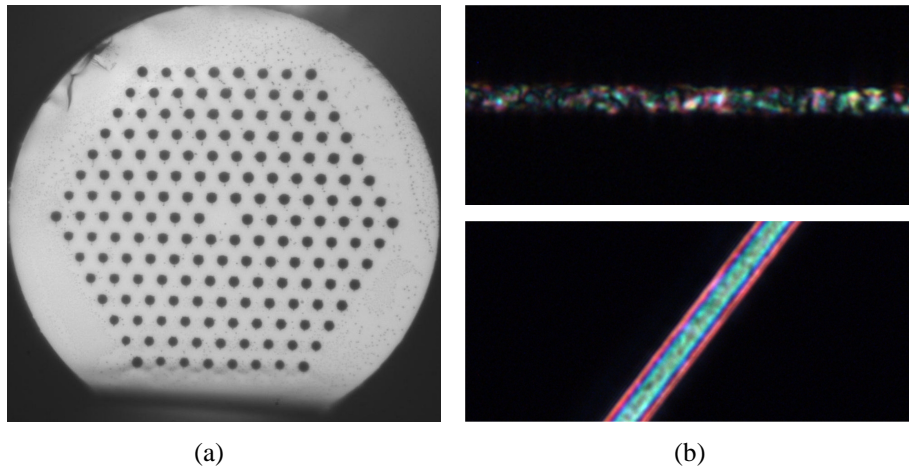


Fig. 1. (a) Optical micrograph of the end facet of the PCF used in the experiment. (b) Polarized micrographs of a silica capillary (inner diameter= $5\mu\text{m}$ ) infiltrated with the nematic LC E7. Capillary is angled at  $0$  degrees (top right) and at  $45$  degrees (bottom right) relative to the axis of the polarizer.

In order to stabilize the alignment of the LC, the PCF was infiltrated with the LC in the isotropic phase ( $70^\circ\text{C}$ ). After the infiltration, the LCPCF was heated to  $70^\circ\text{C}$  again and slowly cooled down to room temperature. This process is necessary to achieve a good uniform alignment of the LC, and, thereby, reduce the insertion loss of the device.

### 3. Thermal and spectral properties

The device presented in this article is based on the nematic liquid crystal E7 from Merck, which is a mixture of the four organic compounds [7] shown in Fig. 2. The optical properties of the LCPBG fiber are determined by the alignment and the wavelength dependent refractive indices of the LC and the thermal tuning sensitivity is dependent on the temperature gradient of the refractive indices.

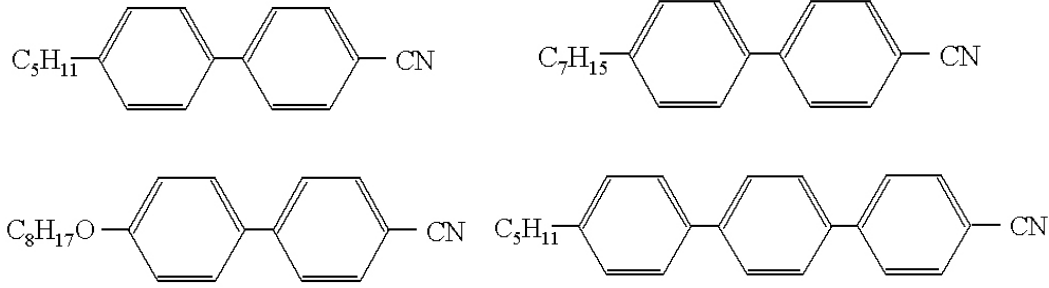


Fig. 2. Molecular structure of the compounds used in nematic LC E7.

The refractive indices as function of wavelength of an anisotropic material can be estimated using the extended Cauchy equations [8]:

$$n_{e,o}(\lambda) = A'_{e,o} + \frac{B'_{e,o}}{\lambda^2} + \frac{C'_{e,o}}{\lambda^4} \quad (1)$$

Where  $n_{e,o}$  is the extraordinary and ordinary refractive index of the LC,  $\lambda$  is the wavelength and  $A'_{e,o}$ ,  $B'_{e,o}$  and  $C'_{e,o}$  are the modified Cauchy coefficients, which can be determined by polynomial fitting to experimental data points. The temperature dependence of the refractive indices can be estimated using a four-parameter model [9]:

$$n_e(T) = A - BT + \frac{2(\Delta n)_o}{3} \left(1 - \frac{T}{T_c}\right)^\beta \quad (2)$$

$$n_o(T) = A - BT - \frac{(\Delta n)_o}{3} \left(1 - \frac{T}{T_c}\right)^\beta \quad (3)$$

Here  $T_c=58^\circ\text{C}$  and is the clearing temperature of the LC,  $A$  and  $B$  are fitting parameters and can be calculated from the temperature dependence of the average refractive index:

$$\langle n(T) \rangle = A - BT \quad (4)$$

where  $\langle n(T) \rangle$  is the average refractive index.  $(\Delta n)_o$  is the birefringence in the crystalline state and the exponent  $\beta$  is a material constant. These parameters can be calculated from the temperature dependence of the birefringence:

$$\Delta n(T) = (\Delta n)_o \left(1 - \frac{T}{T_c}\right)^\beta \quad (5)$$

Using these equations and experimental data points measured, with a “Multi-wavelength Abbe Refractometer”, Atago model DR-M4, from  $15^\circ\text{C}$  to  $55^\circ\text{C}$  in steps of  $5^\circ$  and at

wavelengths 450nm, 486nm, 546nm, 589nm, 633nm and 656nm, it is possible to calculate the refractive indices at any optical wavelength and temperature. Figure 3 shows the wavelength dependent refractive indices for  $T=15^{\circ}\text{C}$  and  $T=55^{\circ}\text{C}$ , where the experimental data points have been used to determine the Cauchy coefficients, which are used to calculate the refractive indices in the near-infrared region. Figure 4 shows the temperature dependent refractive indices measured at  $\lambda=450\text{nm}$  and  $\lambda=656\text{nm}$ .

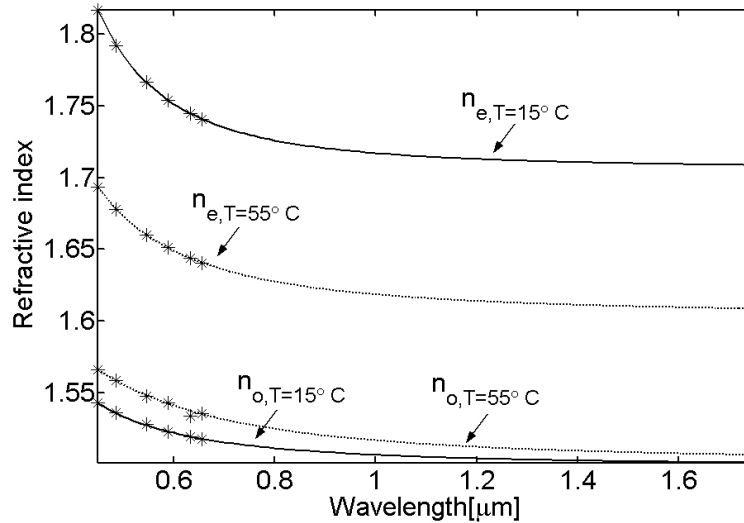


Fig. 3. Ordinary and extra-ordinary refractive indices as function of wavelength of nematic LC E7. The experimental points have been measured using a “Multi-wavelength Abbe refractometer” (Atago model DR-M4) and the theoretical curves have been calculated using the extended Cauchy equations for anisotropic materials.

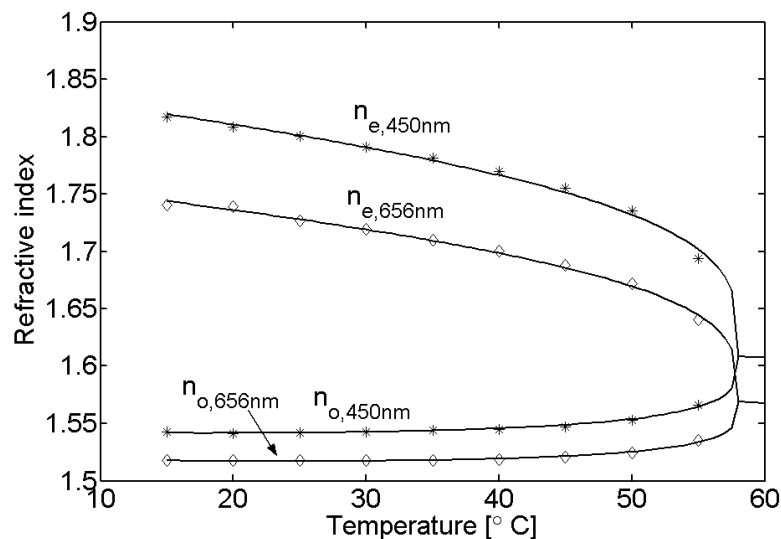


Fig. 4. Ordinary and extraordinary refractive indices as function of temperature of nematic LC E7. The experimental points have been measured using a “Multi-wavelength Abbe refractometer” (Atago model DR-M4) and the theoretical curves have been calculated using the four parameter model.

The infiltration of the air holes with the LC changes the waveguiding properties of the infiltrated section, since the fiber now has a low-index core surrounded by high-index anisotropic rods. The infiltrated section cannot guide by mTIR, but can support a number of guided wavelength bands due to anti-resonant reflection from the LC-filled holes. If the refractive indices of the LC are considerably higher than that of silica, the LC infiltrated holes can be approximated as being isolated waveguides and the spectral position of the bandgaps becomes insensitive to the inter hole distance. In this case, the spectral features of the fiber can be estimated using a simple cut-off approach, where minima in the transmission spectrum occur at cut-off wavelengths of the optical modes supported by one LC filled hole [10,11,12]. In the isotropic case, this is fairly simple, and the transmission minima are approximately given by the simple analytical expression [11]:

$$\lambda_m = \frac{2d}{m + \frac{1}{2}} \sqrt{n_2^2 - n_1^2} \quad (6)$$

Here  $\lambda_m$  is the wavelength of transmission minima,  $d$  is the diameter of the hole,  $m$  is an integer,  $n_2$  is the refractive index of the isotropic liquid filling the hole/core and  $n_1$  is the refractive index of the cladding material, which in this case is silica with  $n_1 \approx 1.45$ . This approach is valid when the individual LC filled holes can be approximated as isolated waveguides. This condition can be written as [11]:

$$\frac{\lambda}{d} \leq 2\sqrt{n_2^2 - n_1^2} \quad (7)$$

The wavelengths given by Eq. (6) are the cut-off wavelengths of the individual LC rods and should coincide with the long-wavelength bandgap edges of the transmission spectrum. Figure 5 shows the calculated average refractive index of E7 at 67°C (isotropic phase). The wavelength dependent refractive indices at this temperature have been calculated using the Cauchy equations and the four-parameter model. Figure 6 shows the experimentally measured transmission spectrum of the LCPBG fiber at  $T = 67^\circ\text{C}$  and the vertical lines mark the long-wavelength side of the bandgaps according to Eq. (6), where the wavelength dependent refractive index of both E7 and silica has been used. As seen, there is good correspondence between the experimental spectrum and theoretical predictions.

Further, in the isolated waveguide regime, the spectral features of the transmission spectrum are predominantly determined by the features of the first inner rings of LC filled holes surrounding the core, but better transmission is achieved when increasing the number of rings [10]. This simple approach gives reasonably good and intuitive results for the isotropic case, but for the anisotropic case it becomes more complicated due to anisotropic splitting of the bands and coupling between the LC waveguides. In the nematic phase, which is an anisotropic phase,  $n_2$  of eq. (7) becomes smaller due to the planar alignment of the LC. This means that the isolated waveguide regime is still valid in the visible region of the spectrum, but the LC waveguides approaches a coupled waveguide regime in the near infrared region, due to a further reduced index contrast in this region. Further, since the LC waveguides are now anisotropic, the optical modes that were coinciding in the isotropic phase start to split-up since the different classes of optical modes (TE, TM, HE, EH) have different z-components of the E-field. This makes the band diagram somewhat more complicated, but a reasonably good agreement between calculated cut-off wavelengths of an anisotropic cylindrical waveguide and experimental data can still be obtained, if we ignore cut-off wavelengths that are closely spaced, since no bandgap guidance is supported when the band separation is narrow. The cut-off wavelengths have been determined by analytically solving Maxwells equations for an anisotropic cylindrical waveguide. Figure 7 shows the transmission spectrum of the LCPBG fiber, when the LC is in the nematic phase at 40 °C. The dotted red lines indicate the cut-off wavelengths of a single LC infiltrated hole with planar aligned LC and, therefore, an



anisotropic rod. The numerically calculated cut-off wavelengths are in agreement with experiments at short wavelengths but as the wavelength is increased, the cut-off wavelengths start to deviate slightly. This is probably because the index contrast of the LC waveguide is decreased and the modes becomes less confined and, therefore, starts to be coupled, and the isolated waveguide approximation can no longer be used.

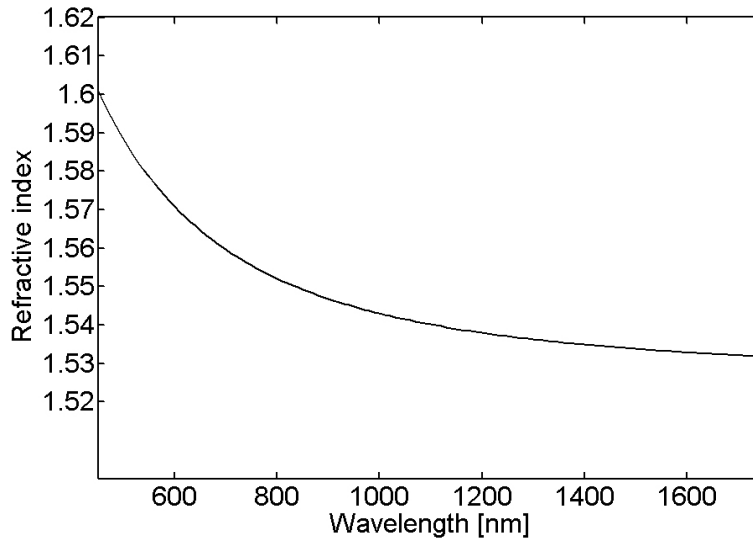


Fig. 5. Calculated average refractive index at 67°C (isotropic phase) of nematic LC E7. The refractive index has been calculated from the experimental data in the nematic phase using both the extended Cauchy equations and the four-parameter model.

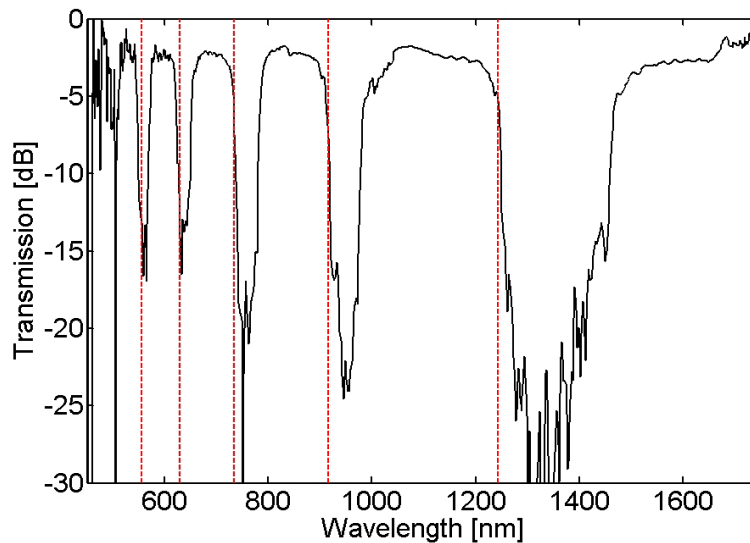


Fig. 6. Transmission spectrum of the LCPBG fiber measured at 67°C (solid black line), which is the isotropic phase of the LC. The PCF was infiltrated for 10mm of the length with the nematic LC E7. The spectral position of the long-wavelength side of the bandgap edges was calculated using a simple analytical expression for the cut-off wavelengths. These are marked with the vertical red dotted lines.

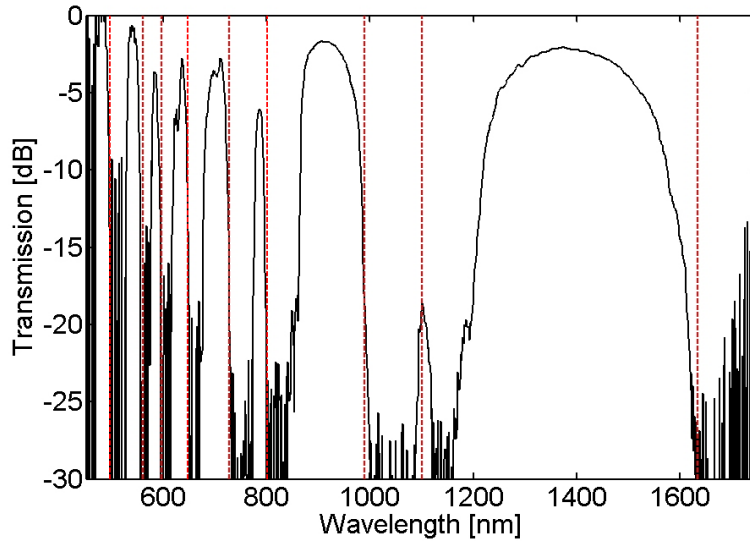


Fig. 7. Transmission spectrum of the LCPBG fiber measured at 40°C (solid black line), which is in the nematic phase of the LC. The PCF was infiltrated for 10mm of the length with E7. The spectral position of the long-wavelength side of the bandgap edges was calculated numerically using a simple cut-off approach for an anisotropic cylindrical waveguide. These are marked as the vertical red dotted lines.

Since the spectral positions of the bandgaps are dominated by the ordinary refractive index, the tuning sensitivity is, therefore, mainly linked to the temperature gradient of  $n_o$ . The cross-over temperature of E7, i.e., the temperature at which the temperature gradient of  $n_o$  is zero, is approximately 21°C, and from Fig. 4 it can be observed that the temperature gradient of  $n_o$  becomes positive, when the temperature is increased to above the cross-over temperature.

Figures 8 and 9 show the temperature dependence of the bandgaps centered at around 545nm and 1400nm of Fig. 7, respectively. The spectra were measured using an unpolarized halogen-tungsten whitelight source and the temperature was controlled using a Linkam MC60 hotplate. The figures clearly illustrate that the tuning sensitivity is increased when the temperature approaches the clearing temperature of the LC (58°C), due to an increasing temperature gradient of  $n_o$ .

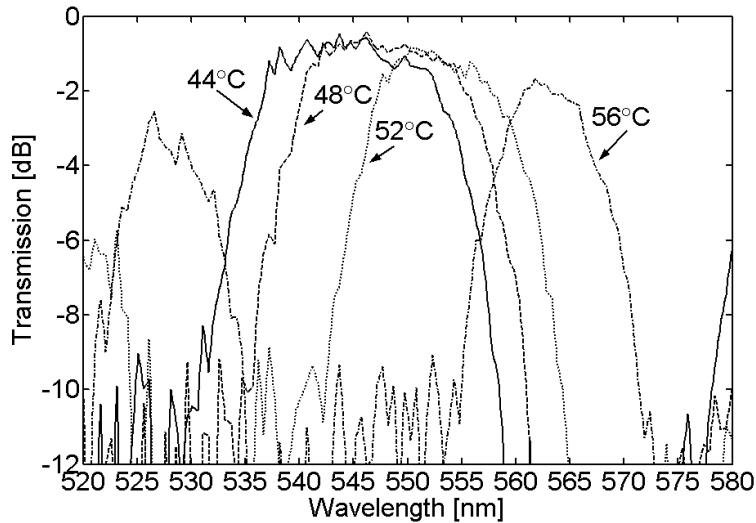


Fig. 8. Thermal tuning of a bandgap located around 545nm. The spectral position of the bandgap is tuned by varying the temperature from 44°C to 56°C, which is just below the clearing point of the LC (58°C). The tuning sensitivity is mainly linked to the refractive index gradient of the ordinary refractive index  $n_o$ . Around room temperature, this gradient is close to zero and only a small tuning sensitivity is observed.

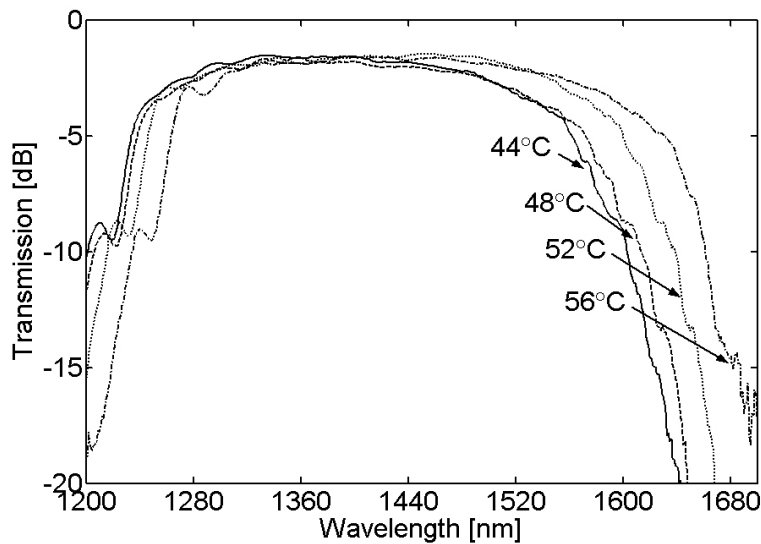


Fig. 9. Thermal tuning of a bandgap located around 1400nm. The spectral position of the bandgap is tuned by varying the temperature from 44°C to 56°C, which is just below the clearing point of the LC (58°C). The tuning sensitivity is mainly linked to the refractive index gradient of the ordinary refractive index  $n_o$ . Around room temperature, this gradient is close to zero and only a small tuning sensitivity is observed.

#### 4. Loss mechanisms

The mechanisms contributing to the transmission losses in the PBG guided modes can be divided into absorption and scattering losses, leakage loss, and mode mismatch and reflection losses. The absorption and scattering losses of nematic LC are generally much larger than that

of silica, and the material loss of silica can, therefore, be ignored. In general, the dominating loss mechanism in bulk nematic LC is scattering losses of around 15-40dB/cm [13], and absorption losses at visible and near-infrared wavelengths are usually very small compared to the scattering loss. Further, it has been shown, that the scattering loss of nematic LCs can be decreased substantially by confining the LC in small capillaries with inner diameters of 2-8 $\mu$ m, and losses of 1-3dB/cm have been reported [14]. Further, the scattering loss of LC capillaries is influenced by the filling technique. For example a higher loss is observed when the capillary is filled using high-pressure than when filling using capillary forces [14]. Leakage loss arises since the cladding structure is finite and the guided mode may penetrate the microstructured cladding and leak into the outer cladding region. The leakage loss is strongly dependent on the number of rings surrounding the core [15]. Losses originating from mode mismatch and reflection losses are minimal in fibers with structural parameters considerably larger than the wavelength. The effective area of the index-guiding section and the PBG guiding section of the fiber are in both cases slightly larger than  $\Lambda^2$  ( $\Lambda$ =inter hole distance) [12, 16], but a small coupling-loss can still be observed because the mode-profiles are not completely identical. Further, reflection losses due to mismatch of the effective index of the index-guiding and PBG guiding mode are also minimal, since the effective indices in both cases are just below the index of silica [17]. This means, that these devices can be inserted into an existing telecom transmission link without any significant degradation, since the mode field diameter can easily be matched to that of a SMF28 and additional reflection losses from the infiltrated section are also avoided since the effective mode index of the infiltrated and non-infiltrated PCF are almost equal. The minimum insertion loss of the nematic LCPBG fibre used in this paper can be determined from Figs. 8 and 9, which shows an insertion loss of 0.5dB and 1.6dB at 540nm and 1400nm, respectively.

## 5. Optical tuning of the LCPBG fiber

It is evident from Figs. 8 and 9 that the transmission properties of the LCPBG fiber can be easily tuned by varying the temperature of the infiltrated section of the fiber, but this is inherently a rather slow process. Therefore, in order to decrease the thermal response time, compared to heating/cooling the entire fiber, a 532nm pulsed laser is used to locally heat the LC positioned in the inner rings of holes surrounding the core. The transfer of energy from the pump to the LC is achieved by doping the LC with an azobenzene dye called Disperse Red 1 (0.4wt%). The dye DR1 has an absorption peak around 502nm and the molecular structure of DR1 is shown on Fig. 10.

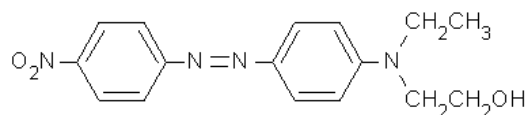


Fig. 10. Molecular structure of Disperse Red 1.

The dye doping does not affect the alignment of the LC, and Fig. 11 shows the bandgaps of the LCPBG fiber before and after dye doping. The figure clearly shows that the presence of the dye, decreases the transmission in the bandgaps located around the dye absorption peak, but does not alter the position or the transmission level of the remaining bandgaps.

The 532nm laser source is coupled into the core of the PCF, such that there is an evanescent field overlapping with the dye-doped LC in the cladding, when the LCPBG fiber supports a guided mode at this wavelength, i.e., a bandgap is present at 532nm. The energy transfer efficiency is increased substantially when there is a high overlap between the core mode and the inner rings of cladding holes. This is achieved by heating the entire fiber using a hotplate, such that the 532nm source is positioned on the edge or just outside a bandgap. On the bandgap edges, the effective area of the core mode increases substantially [17], thereby leading to a higher overlap between the core mode and the LC in the inner rings of holes. As

seen from Fig. 8, the 532nm laser will be positioned on the bandgap edge or outside a bandgap when the LC temperature is between 44°C and 56°C.

In order to investigate the dynamics of the LCPBG fiber device, a low-power CW probe laser was coupled into the fiber together with the pulsed pump laser. Both the polarization of the pump and the probe could be individually adjusted using the setup shown on Fig. 12. The probe laser was chosen to be located on the long-wavelength side of the bandgap centered at around 1400nm, i.e., at 1620nm due to the availability of a laser source in this range.

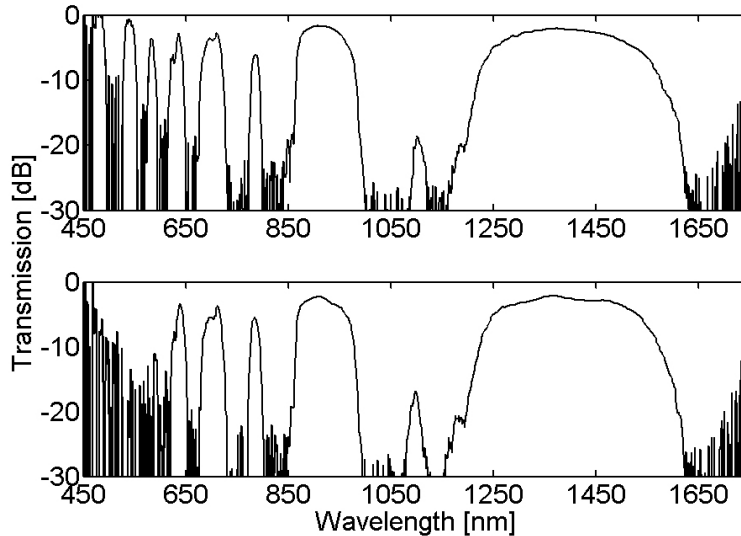


Fig. 11. Doping the LC with the dye Disperse Red 1 (DR1), enhances the absorption around 500nm, but does not alter the alignment and the transmission above the absorption wavelengths of the dye. Transmission spectra with an un-doped LC (top), and a doped LC (bottom).

The temperature of the LCPBG fiber was raised to 45°C and the probe laser was monitored using a PIN photo detector and a storage oscilloscope. The pulsed pump laser (square-wave modulated, 50% duty cycle) was turned on and the polarization of both the pump and probe laser was adjusted until a modulation of the probe laser was observed on the oscilloscope. Figure 13 shows the observed waveforms of the 1620nm probe laser when the 532nm pump laser was modulated with 100Hz, 1kHz and 2kHz square wave signal. During the pump pulse, the LC is heated and the ordinary refractive index of the LC increases, which causes the bandgaps to shift toward longer wavelengths. This modulates the power of the probe laser, which is located on the edge of the bandgap. An explanation for the modulation ripples on Fig. 13(a) was not found. The pump power was monitored and we estimate that the power of the pump coupled into the LCPBG device, at the junction of the butt-coupling indicated in Fig. 12, was around 2-3mW. Increasing the input power did not yield any improvement, which is attributed to a too large increase in temperature, whereby a bandgap shift up in wavelength and assist in confining the 532nm pump to the core region, and thereby decreasing the effective area of the core mode and, thereby, also decreasing the overlap with the LC.

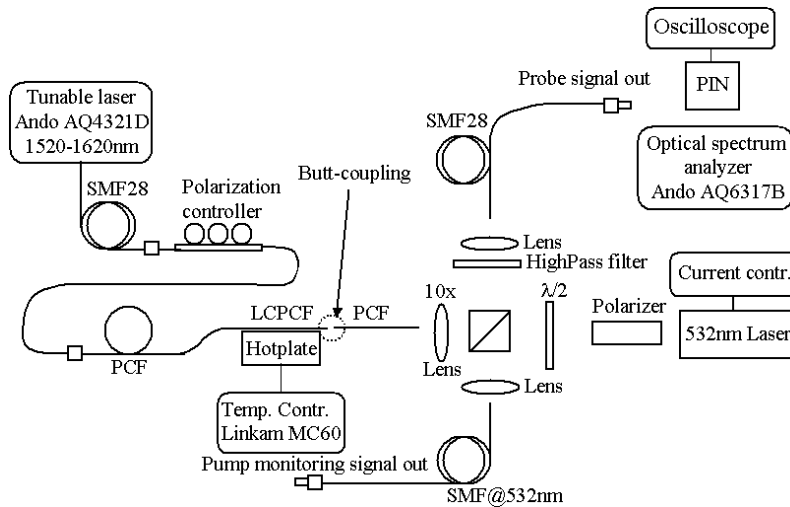


Fig. 12. Experimental setup for measuring the dynamics of the dye-doped LCPBG fiber. The same setup is used for measuring the polarization sensitivity of the bandgaps.

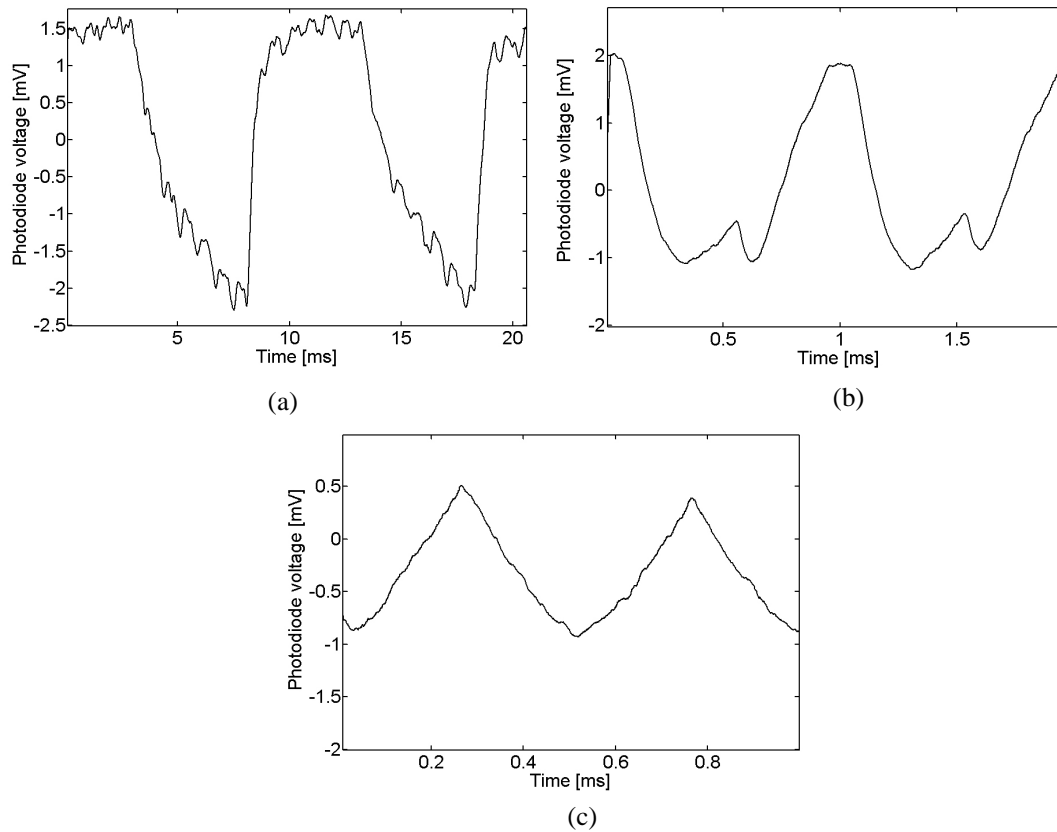


Fig. 13. Oscilloscope traces of the time-domain response of the 1620nm CW polarized laser source, which is coupled into the dye-doped LCPBG fiber. The traces show the response of the 1620nm CW source when the pump laser is square-wave modulated with  $f=100\text{Hz}$  (a),  $f=1\text{kHz}$  (b) and  $f=2\text{kHz}$  (c). The estimated pump power was 2-3mW.

## 6. Polarization properties

Toward the center of the bandgap, no polarization sensitivity of the transmission level was observed, while this was not the case on the edge of the bandgap. Using a polarized tunable laser, we measured the polarization sensitivity of the bandgap edge from 1520-1620nm and observed a small shift (approx. 10-15nm) of the bandgap edge depending on the polarization of the laser. This shift is attributed to very small variations (few tens of nanometers) in the hole diameter and shape of the inner ring of holes, thereby leading to a small birefringence.

Figure 14 shows the transmission spectrum of the LCPBG fiber device measured at 40°C with a polarized laser source. The polarization sensitive bandgap shift was measured using two polarizations, Polarization 1 and Polarization 2. These polarizations were identified by maximizing and minimizing the power at 1620nm, respectively. It should be expected that this polarization sensitivity should cause birefringence near the bandgap edges, since the two polarization modes have different effective mode indices. Also, it would be interesting to know if this resulted in any noteworthy birefringence toward the center of the bandgap.

The Differential Group Delay (DGD), which is the time delay between the two Principal States of Polarization (PSP), of the LCPBG fiber was, therefore, measured using the HP/Agilent 8509 Polarization Analyzer and the HP 8168C tunable laser source. Figure 15 shows the DGD measured from 1520-1600nm at different temperatures. The DGD is around 0ps toward the center of the bandgap, but increases slightly toward the bandgap edge. A temperature sensitivity of the DGD is observed, which is caused by the temperature sensitivity of the spectral location of the bandgap. Further, it should be mentioned the DGD is very low but the corresponding birefringence  $\Delta n = \text{DGD} \cdot c / L = 0.07 \text{e-}12 \cdot 3 \text{e}8 / 10 \text{e-}3 = 2 \text{e-}3$  is rather high and comparable to birefringence in polarization maintaining PCFs [18,19].

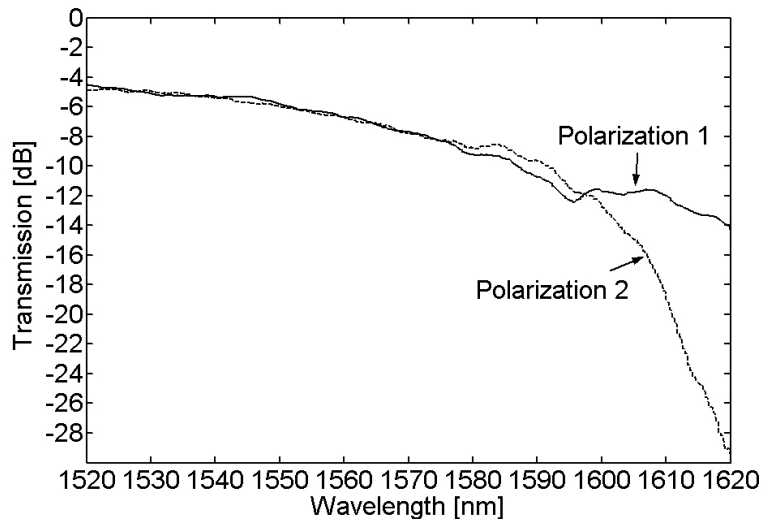


Fig. 14. Polarization sensitivity of the transmission at the edge of the bandgap centered around 1400nm in Fig. 7. Maximizing and minimizing the transmission at 1620nm identified polarization 1 and Polarization 2, respectively.

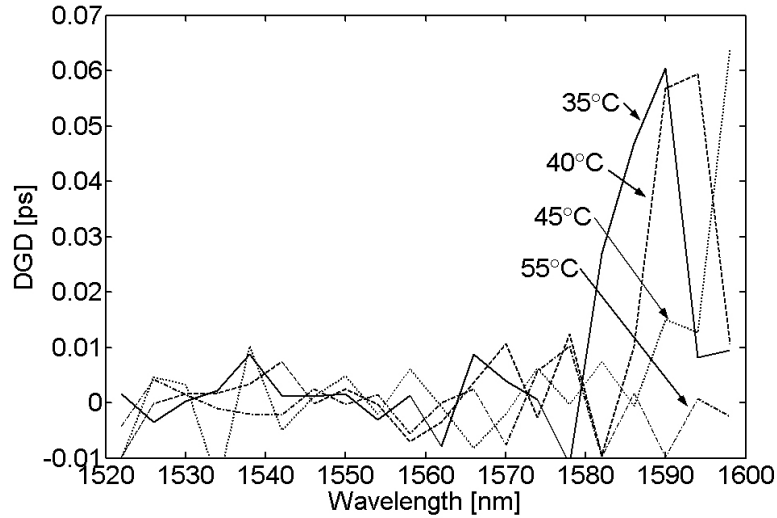


Fig. 15. Differential Group Delay (DGD) measured on the LCPBG fiber with the polarization sensitive bandgap edges shown on Fig. 14. The DGD was measured using the HP/Agilent 8509 Polarization analyzer and the HP 8168C tunable laser. A relatively small temperature sensitive DGD is measured on the edge of the bandgap, but due to the short length of the LCPBG fiber, this translates into a rather high birefringence on the order of  $10^{-3}$ .

## 7. Dynamics

The rise time of the 1620nm modulated signal, measured from 10% to 90% amplitude modulation, was estimated to be 190 $\mu$ s, 250 $\mu$ s and 400 $\mu$ s, for pulse durations of 250 $\mu$ s, 500 $\mu$ s and 5ms, respectively. The optical response to the different modulation frequencies was not measured on the same sample, which means that small variations in hole size and shape along the fiber can cause the slope of the bandgap edge to vary between the samples. Therefore, exact comparison of rise and decay times at different frequencies should not be made. The rise time is linked to the thermalization time, i.e. the timescale on which the absorbed optical energy is transferred from the dye to the LC. The thermalization time is around 1-10ns, but the response time is further limited to 100-200ns by the viscous forces, since the thermo-optic effect is directly linked to the temperature dependence of the order parameter [20], i.e., the directional order of the LC. Further, a slowing down behavior of the order parameter is observed near the nematic to isotropic phase transition temperature, which further reduces the response time [20]. The dynamics of the decay time can be divided into two regimes in which different decay times can be observed: a long-pulse regime and a short-pulse regime, which relates the duration of the pulse to the thermal diffusion time,  $\tau_{TD}$ , of the LC rods. The decay time, also measured from 90% to 10% modulation, was estimated to be 175 $\mu$ s, 120 $\mu$ s and 3.2ms, for pulse durations of 250 $\mu$ s, 500 $\mu$ s and 5ms, respectively. Again an exact comparison between the decay times should not be made, but it is evident that for a pulse duration of 5ms, the decay time is an order of magnitude longer than for the short pulses. This is due to a change in the characteristic length scale in the thermal diffusion process. The thermal diffusion time,  $\tau_{TD}$ , can be written as [21]:

$$\tau_{TD} = \frac{C_p \rho}{\lambda_T} L^2 \quad (8)$$



Where  $C_p$  is the heat capacity,  $\rho$  is the material density,  $\lambda_T$  is the heat conductivity and  $L$  is the characteristic diffusion length scale. For a LC rod with  $3\mu\text{m}$  diameter,  $C_p=2\text{J/gK}$ ,  $\rho=1\text{g/cm}^3$  and  $\lambda_T=16\cdot 10^{-4}\text{ J/cmsK}$  [22], the thermal diffusion time is  $\tau_{\text{TD, LC}} \approx 100\mu\text{s}$ . For comparison, the silica area between three LC rods has  $\tau_{\text{TD, SiO}_2} \approx 20\mu\text{s}$  ( $C_p=0.7\text{J/gK}$ ,  $\rho=2.2\text{g/cm}^3$ ,  $L=4\mu\text{m}$  and  $\lambda_T=14\cdot 10^{-3}\text{ J/cmsK}$ ). Therefore, when the LC rods are heated with a pulse, which has a time duration considerably longer than  $\tau_{\text{TD, LC}}$ , the LC will heat up, thereafter, the thermal energy in the LC will be transferred to the silica, which also heats up. At the end of the pulse, the pump pulse has heated both the LC and the silica. Therefore, in order to link the decay time to  $\tau_{\text{TD, LC}}$ , it is necessary to increase the characteristic diffusion length in Eq. (8), since the heated volume is much larger in this regime. Assuming that the first three rings of LC rods are heated by the pump pulse i.e.  $L \approx 40\mu\text{m}$  and assuming that the effective values of  $C_p$ ,  $\rho$  and  $\lambda_T$ , are the values of silica and the LC weighted with the LC filling fraction of the PCF structure ( $f_{\text{LC}}=18\%$ ), the thermal diffusion time of the mixed material structure  $\tau_{\text{TD, SiO}_2+\text{LC}} = 2.5\text{ms}$ , which is close to the observed decay time of  $3.2\text{ms}$ . In the short pulse regime,  $\tau_{\text{TD, LC}} \approx 100\mu\text{s}$ , which is in good agreement with the decay times of  $175\mu\text{s}$  and  $120\mu\text{s}$  measured at pulse durations of  $250\mu\text{s}$  and  $500\mu\text{s}$ , respectively.

From the 100Hz modulation trace in Fig. 13(a), a  $3.5\text{mV}$  modulation amplitude was obtained. Taking into account both the slope of the bandgap edge at Polarization2 and the linear response of the photodetector, we estimate that the spectral shift was approximately  $3\text{-}4\text{nm}$ .

## 8. Conclusion

In this paper we have, to our knowledge, presented the first optically tunable PBG fiber device. We have demonstrated how a  $532\text{nm}$  pulsed laser can modulate a  $1620\text{nm}$  CW laser by locally modifying the optical properties of LC inclusions in a LC infiltrated PCF. This is achieved using a low pump power of only  $2\text{-}3\text{mW}$ , and we have demonstrated a modulation frequency of up to  $2\text{kHz}$ . We have analyzed the thermal and spectral characteristics of the device, and we have measured an insertion loss of  $0.5\text{dB}$  at  $540\text{nm}$  and  $1.6\text{dB}$  at  $1400\text{nm}$ .

We have demonstrated that there is a short- and long-pulse regime in which the decay times vary by an order of magnitude. The rise time was of the same order of magnitude in these two regimes. We believe that these optically tuned LCPBG fiber devices can find use as distributed devices i.e. with signal processing elements, such as tunable Bragg gratings, distributed in a transmission fiber and with the data signal (the probe) and the control signal (the pump) carried in the same fiber.

## Acknowledgments

This work was financially supported by the NKT Academy in Denmark. Merck (Darmstadt, Germany) is acknowledged for providing the LC used in these experiments.